

Fracture energy and tension softening relation for nano-modified concrete

A. Ramachandra Murthy^{*}, P. Ganesh^a, S. Sundar Kumar^b and Nagesh R. Iyer^c

CSIR-Structural Engineering Research Centre, Chennai 600113, India

(Received November 1, 2014, Revised March 24, 2015, Accepted April 6, 2015)

Abstract. This paper presents the details of size independent fracture energy and bi-linear tension softening relation for nano modified high strength concrete. Nano silica in powder form has been used as partial replacement of cement by 2 wt%. Two popular methods, namely, simplified boundary effect method of Karihaloo *et al.* (2003) and RILEM (1985) fracture energy with P - δ tail correction have been employed for estimation of size independent fracture energy for nano modified high strength concrete (compressive strength ranges from 55 MPa to 72 MPa). It is found that both the methods gave nearly same values, which is an additional evidence that either of them can be employed for determination of size independent fracture energy. Bi-linear tension softening relation corresponding to their size independent fracture energy has been constructed in an inverse manner based on the concept of non-linear hinge from the load-crack mouth opening plots of notched three-point bend beams.

Keywords: high strength concrete; nano-silica; size dependent fracture energy; size independent fracture energy; tension softening relation

1. Introduction

For the analysis of cracked concrete structural components, two mechanical properties, namely, the specific fracture energy of concrete and the corresponding tension softening relation are the most important properties. It is well known that the work-of-fracture method recommended by RILEM (1985) for measuring the specific fracture energy of concrete from notched three-point bend specimens of different sizes and notch to depth ratios is still the most common method despite the fact that the specific fracture energy so measured is known to vary with the size and shape of the test specimen (Bazant and Kazemi 1991, Bazant 1996, Nallathambi *et al.* 1985, Carpinteri and Chiaia 1996, Hu and Wittmann 1992, Mindess 1984, Pan 2011, Sahin and Koksal 2011). The reasons for the variation of fracture energy are known for nearly two decades. From the literature, it is observed that there two popular methods, namely, RILEM work of fracture method

*Corresponding author, Scientist, E-mail: murthyarc@serc.res.in

^aSenior Research Fellow

^bScientist

^cFormer Director

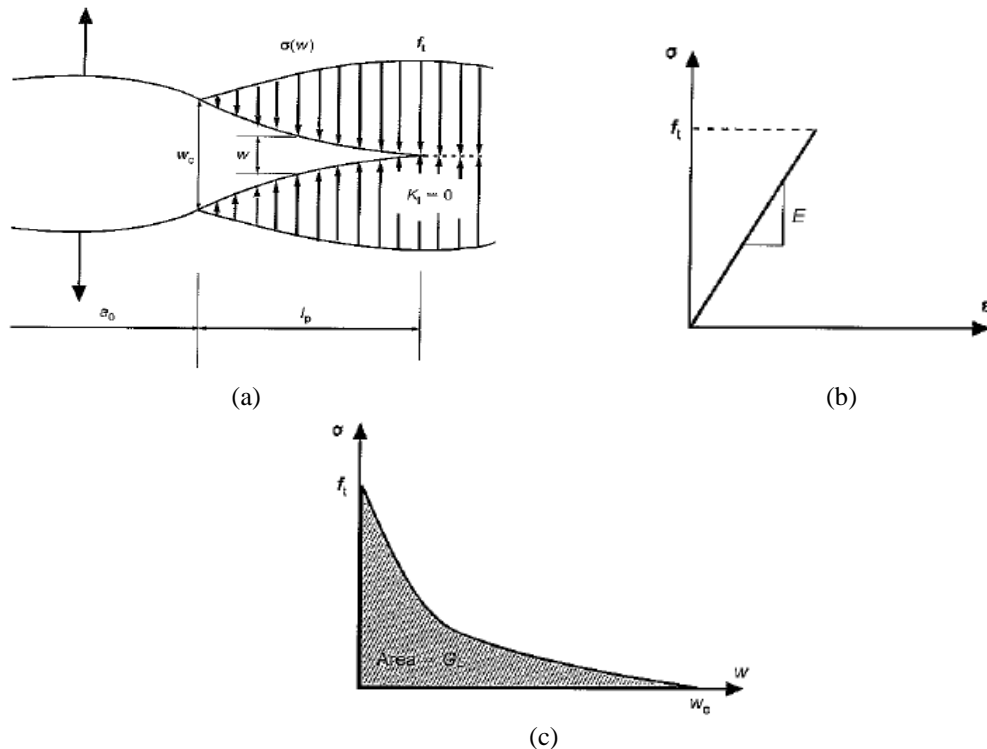


Fig. 1 (a) A real traction-free crack of length a_0 terminating in a fictitious crack of length l_p whose faces close smoothly near its tip ($K_I=0$), (b) The material ahead of the fictitious crack tip is assumed to be linear, (c) The material within the fracture process zone is softening; the area under softening curve equals fracture energy (Karihaloo 1995)

with P - δ tail correction due to Elices and co-investigators (Elices *et al.* 1992, Guinea *et al.* 1992, Planas *et al.* 1992) and boundary effect method due to Hu and Wittmann (2000). Elices and co-investigators (Elices *et al.* 1992, Guinea *et al.* 1992, Planas *et al.* 1992) identified the sources of experimental error in the RILEM method and proposed a methodology for eliminating the major source of error, namely by including the work-of-fracture that is not measured in the RILEM method due to practical difficulties in capturing the tail part of the load-deflection plot. The second method proposed by Hu and Wittmann (2000) recognized that the local specific energy varied during the propagation of a crack, the variation becoming more pronounced as the crack approached the stress-free back face boundary of the specimen. Karihaloo *et al.* (2003) and Abdalla and Karihaloo (2003) extended the free boundary effect concept of Hu and Wittmann (2000) and showed that the same size-independent specific fracture energy can also be obtained by testing only two specimens of the same size but with notches which are well separated. Their method greatly reduces the number of test specimens and simplifies the determination of size independent fracture energy. Recently, the first of its kind, Cifuentes *et al.* (2013) showed that if the size-dependent G_f measured by the RILEM method is corrected following the above methods or its simplification proposed by Karihaloo *et al.* (2003), if the notch to depth ratios are well separated, then the resulting specific fracture energy G_F is very nearly the same and independent of the size of the specimen. This conclusion was arrived at on the basis of a limited set of results on a

single concrete mix of compressive strength 37 MPa. Later Ramachandra Murthy *et al.* (2013) demonstrated that the size independent fracture energy obtained by using above two methods for compressive strength ranging in 57 MPa to 120 MPa gave nearly same value.

The non-linear theory of fracture mechanics based on the fictitious crack model is generally employed for the analysis of cracked concrete structures (Hillerborg 1976). Hillerborg model is based on the fact that an extensive fracture process zone (FPZ) exists ahead of a real traction-free crack in which concrete softens progressively due to micro-cracking and other energy dissipation processes. This tension softening FPZ is included in the model as a fictitious crack (or a cohesive zone), which means that this portion of the crack cannot be continuous with full separation of its faces, as in a real traction-free crack. Under mode I loading, the residual tensile stress increases from zero at the tip of a real traction-free crack to the full uni-axial tensile strength of concrete at the tip of the fictitious crack (Fig. 1). For the fictitious crack model (FCM), two material properties of concrete, namely, the specific fracture energy, G_F , and the corresponding tension softening relationship $\sigma(w)$ relating the residual stress transfer capacity σ to the opening displacement w of the fictitious crack faces are needed in addition to its tensile strength f_t and Young's modulus, E . In practice, the $\sigma(w)$ relationship is generally assumed as linear, bilinear, multi-linear or even an exponentially decaying curve with the bilinear approximation being the most common (Karihaloo 1995). The significance of the bilinear approximation of the tension softening diagram (TSD) stems from the fact that it captures the two major mechanisms responsible for tension softening in concrete, namely micro-cracking and frictional aggregate interlock.

Within the last few decades, Testing of discrete macro to micro-fibers to control cracking and crack propagation in plain concrete, and to increase the overall ductility of the material is in progress. The development of particles at the nanoscale has opened a new field of research in concrete. Nanotechnology is a emerging avenue and has an potential improvement in properties of concrete in fresh and hardened state. Nanotechnology encompasses the techniques of manipulation of the structure at the nanometer scale to develop a new generation of tailored, multifunctional, cementitious composites with superior mechanical performance and durability potentially, having a range of novel properties such as low electrical resistivity, self-sensing capabilities, self-cleaning, self-healing, high ductility, and self-control of cracks. Concrete can be nano-engineered by the incorporation of nano-sized building blocks or objects (e.g., nanoparticles and nanotubes) to control material behaviour and add novel properties (Pacheco-Torgal and Said Jalali 2011, Sanchez and Sobolev 2010, Singh *et al.* 2013, Said *et al.* 2012, Mostafa Jalal 2014, Ramin Tabatabaei *et al.* 2014). Recently fracture properties of high performance concrete containing nano silica are investigated by Zhang *et al.* (2014) with various proportion of steel fibres in it.

Study on fracture behaviour of nano modified concrete is found be very limited. In this paper, an experimental evaluation of size independent specific fracture energy and corresponding tensile stress vs crack width relation for nano modified high strength concrete has been carried out. This paper showed further evidence that both methods yield more or less a unique value of size independent fracture energy and the corresponding tension softening relation can be deduced accordingly.

2. Determination of size independent fracture energy

It is known that there are two popular test methods, namely, RILEM work of fracture method

with P - δ tail correction and boundary effect method to determine size independent fracture energy. Brief details of the methods are presented.

2.1 Method proposed by Elices *et al.* (P - δ tail)

Elices and co-investigators (Elices *et al.* 1992, Guinea *et al.* 1992, Planas *et al.* 1992) identified several sources of energy dissipation that influence the measurement of G_f by the RILEM work-of-fracture method. Most of these sources are due to experimental errors and the sources of errors are classified into three main groups, namely, (i) the testing equipment and experimental setup, (ii) the energy dissipation in the specimen bulk, and (iii) the non-measured energy corresponding to the un-recorded tail of the load-deflection (P - δ) curve near the end of the test. The first source of error can be avoided with a proper calibration of the equipment and design of supports and loading system. The second source is due to crushing at supports and under the loading point, and due to high tensile stresses in the specimen bulk. The crushing dissipation can be corrected by adjusting the initial stiffness of the P - δ curve and measuring the mid-span deflection on the lower half of the beam depth. The dissipation in the specimen bulk, W_{db} , due to high tensile stresses cannot be avoided; however, it was estimated that this causes an error of less than 2%. The last source of error is due to the curtailment of the tail of the P - δ near the end of the test due to practical difficulties of unloading the cracked specimen fully in a stable manner and it is found that it has the most significant effect on the size dependency of the measured fracture energy. To estimate this non-measured energy when the test is stopped ($W_{nm}=W_{nm1}+W_{nm2}$ in Fig. 2) at a very low load, it is necessary to model the beam behaviour when the crack is close to the free surface (Elices *et al.* 1992). The size-independent specific fracture energy of concrete can be calculated as (Elices *et al.* 1992)

$$G_F = \frac{\int_0^{\delta_u} Pd\delta + W_{nm}}{b(D-a)} \quad (1)$$

where,

- $b(D-a)$ = Area of the ligament (A_{lig}) of the test specimen that was un-cracked at the start of the test
- b = width of the specimen,
- $Pd\delta+W_{nm}$ = Measured Work of Fracture + Non measured Work of Fracture.

2.2 Boundary Effect Method (BEM)

The effect of stress-free back boundary of the specimen is observed by Hu and Wittmann (1992) in the fracture process zone (FPZ) ahead of a real growing crack. The local fracture energy varies with the width of the fracture process zone and as the crack approaches the back stress-free face of the specimen the fracture process zone becomes more pronounced and hence the local fracture energy decreases. The change in the local fracture energy (g_f) is approximated by a bilinear function, as shown in Fig. 3. The transition from horizontal to the sharply inclined line occurs at the transition ligament length, which depends on the material properties, specimen size and shape. In the boundary effect model of Hu and Wittmann (2000), the measured RILEM fracture energy, G_f , may be considered as the average of the local fracture energy function (dotted

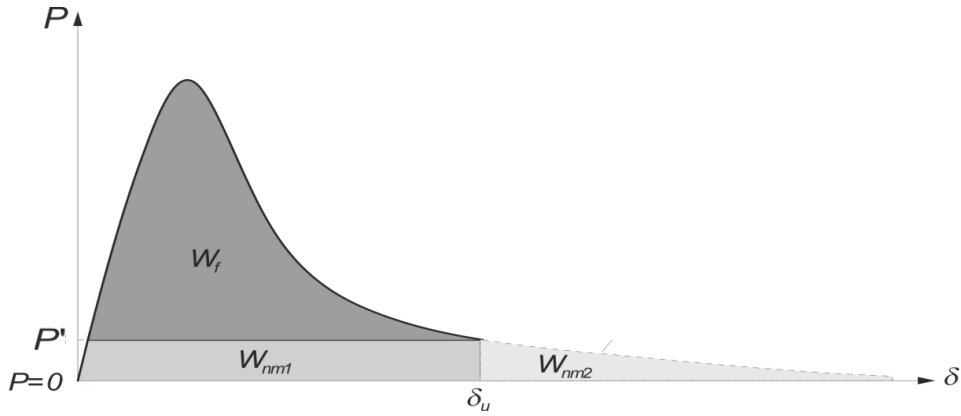


Fig. 2 P - δ curve in a three-point bend test and the measured (W_f) and non-measured ($W_{nm1}+W_{nm2}$) work of fracture

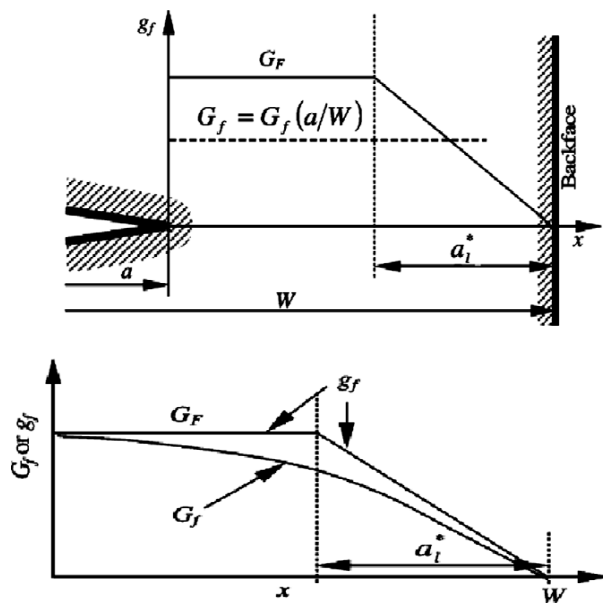


Fig. 3 Variation of local fracture energy g_f and G_F over the ligament length (Karihaloo *et al.* 2003)

line in Fig. 3) over the initial un-cracked ligament area. The relationship between all the associated variables is given by

$$G_f(a,W) = \frac{\int_0^{W-a} g_f(x) dx}{W-a} = \begin{cases} G_F \left[1 - \frac{a_1^*/W}{2(1-a/W)} \right]; & 1-a/W > a_1^*/W \\ G_F \frac{2(1-a/W)}{2a_1^*/W}; & 1-a/W \leq a_1^*/W \end{cases} \quad (2)$$

in which G_f is the specific fracture energy or size dependent fracture energy (RILEM), G_F is the true or size-independent fracture energy, W is the overall depth of the beam, a is the initial notch depth and a_1^* is the transition ligament length.

To obtain the values of G_F and a_1^* of a concrete mix, the size-dependent specific fracture energy G_f of specimens of different sizes and a range of the notch to depth ratios is first determined by the RILEM work-of-fracture method. Then Eq. (2) is applied to each specimen depth and notch to depth ratio. This gives an over-determined system of equations which is solved by a least squares method to obtain the best estimates of G_F and a_1^* .

In the present study, the simplified boundary effect method proposed by Karihaloo *et al.* (2003) has been used to determine the G_F .

3. Bi-linear tension softening relation by cracked hinge concept

In the fictitious crack model, it is assumed that prior to crack initiation from a notch, the material exhibits linear elastic behaviour. After crack initiation, it is assumed that stresses may be transmitted across the fictitious crack faces. These crack bridging forces are taken to be a function of the crack opening displacement given by the stress-crack opening relationship. The bending failure of notched concrete beams may be modelled by the development of a fictitious crack in an elastic layer ahead of the notch. The basic idea of the non-linear cracked hinge model is to isolate the part of the beam close to the propagating crack (i.e., the part under maximum bending moment) as a short beam segment subjected to a bending moment and axial force. Fig. 4 shows a typical notched Three Point Bend (TPB) beam specimen. In the non-linear hinge model the crack is viewed as a local change in the overall stress and strain field. This change is assumed to vanish outside a certain band of width s (Fig. 4). Thus, outside of this band the structural element is modelled using the elastic beam theory. The boundaries of the hinge are assumed to undergo only rigid body rotation and translation. The constitutive relationship for each segment inside the hinge is assumed to be linear elastic in the pre-cracked state (phase 0), while the cracked state is approximated by a bilinear softening curve as shown in Fig. 5

$$\sigma = \begin{cases} E\varepsilon & \text{pre-cracked state} \\ \sigma(w) = g(w)f_t & \text{cracked state} \end{cases} \quad (3)$$

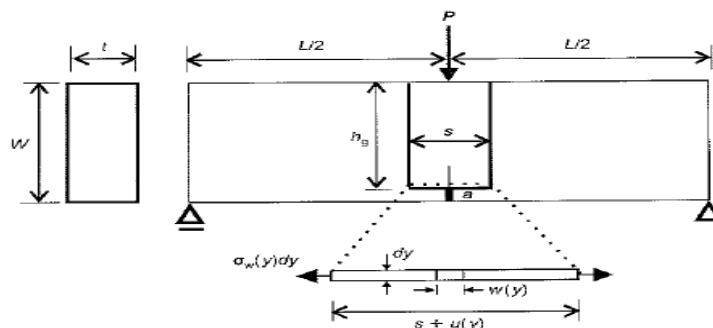


Fig. 4 Three-point notched bend beam with a non-linear hinge modelling the propagation of a crack at mid-section (Abdalla and Karihaloo 2004)

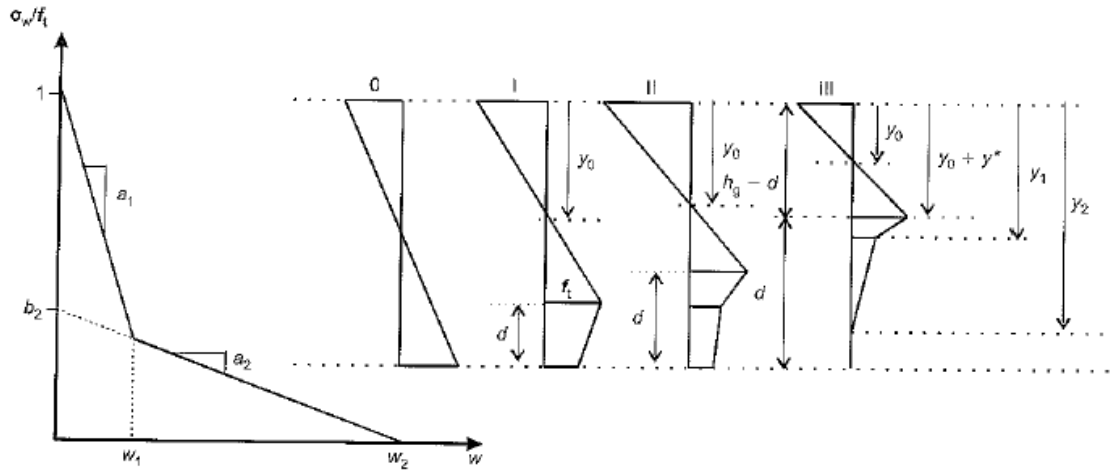


Fig. 5 A bilinear stress-crack opening relationship and the four different phases of crack propagation. Phase 0=state of stress prior to cracking; Phases I-III=states of stress during crack propagation (Ostergaard 2003)

where E is the elastic modulus; ε is the elastic strain; w is the crack opening; f_t is the uniaxial tensile strength; and $g(w)$ is the function representing the shape of the stress-crack opening relationship, normalized such that $g(0)=1$. For the assumed bilinear shape (Fig. 5), we have

$$g(w) = \begin{cases} b_1 - a_1 w, & 0 \leq w \leq w_1 \\ b_2 - a_2 w, & w_1 \leq w \leq w_2 \end{cases} \quad (4)$$

$$w_1 = \frac{1 - b_2}{a_1 - a_2} \quad (5a)$$

$$w_2 = \frac{b_2}{a_2} \quad (5b)$$

where $b_1=1$; and the limits w_1 and w_2 are given by the intersection of the two line segments, and the intersection of the second line segment with the abscissa, respectively (Fig. 5). An analysis of the hinge element allows the determination of the axial load N and bending moment M for any given angular hinge rotation 2φ (Fig. 6). The problem now is solved in four stages, one for each phase of the crack propagation. Phase 0 represents the elastic state, when no crack has formed from the initial notch, while phases I, II and III represent different stages of crack propagation (Fig. 5).

4. Application of hinge model to TPB

The opening displacement TPB specimens consists of parts. These are the opening due to the crack emanating from the starter crack, δ_{COD} , the opening due to elastic deformation, δ_e , and the

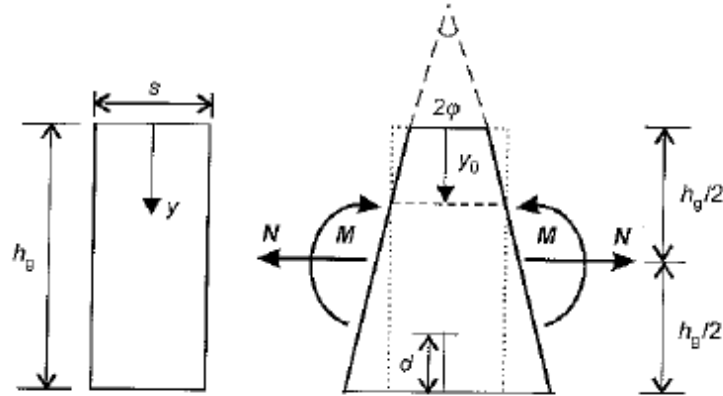


Fig. 6 Geometry, loading and deformation of the hinge element (Abdalla and Karihaloo 2004)

opening due to geometrical considerations because the line of application of the load is shifted relative to the mouth of the starter crack, δ_g

$$CMOD = \delta_{COD} + \delta_e + \delta_g \quad (6)$$

δ_{COD} is the crack opening at the bottom of the crack in the hinge, that is, at $y=h_g$, (Figs. 4 and 6)

$$\delta_{COD} = \frac{sf_t}{E} \frac{(1 - b_i + 2\alpha_h \theta)}{(1 - \beta_i)} \quad (7)$$

where s is the width of the hinge, $ah=d/hg$, $\theta = \mathbf{h}_g \mathbf{E} \varphi / \mathbf{s} \mathbf{f}_t$, φ is half of the hinge rotation and the parameter β_i can be obtained from

$$\beta_i = \frac{sa_i f_t}{E} \quad (8)$$

δ_e in Eq. (6) can be found from handbooks (Tada *et al.* 1985). The contribution from δ_g has been found to be negligible for the specimen geometries tested.

The complete details of inverse analysis and evaluation of bi-linear parameters can be found in literature (Abdalla and Karihaloo 2004, Tada *et al.* 1985, Ulfkjaer *et al.* 1995, Stang and Olesen 1998, Olesen 2001, Ostergaard 2003). But the important point to note is the tension softening diagram and the bi-linear parameters obtained from inverse analysis are corresponding to size dependent fracture energy. The parameters obtained from inverse analysis have been modified as per the procedure given by Abdalla and Karihaloo (2004) so that they correspond to the true G_F of the concrete mix that is independent of the shape and size of the test specimen.

5. Experimental Investigation

Prismatic notched specimens were subjected to three-point bending in accordance with the RILEM procedure (1985). Details of the specimens prepared for experimental study and notch depth details are given in Table 1. The properties of the ingredients used to develop the HSC

Table 1 Geometrical Properties of the notched specimens

Mix	Beam dimension (mm) (length×width×depth)	Notch to depth ratio
HSC 1	250×50×50	0.1
	250×50×50	0.6
HSC 2	250×50×50	0.1
	250×50×50	0.6
HSC 3	250×50×50	0.1
	250×50×50	0.6

Table 2 Properties of ingredients used for HSC mixes

Cement	Grade - 53 (OPC)
	Specific gravity - 3.15 Particle size range - 31 μm to 7.5 μm
Silica fume (SF)	Specific gravity - 2.2 Particle size range- 0.2 to 25 μm Percentage of passing - 92% (45 μm sieve in wet sieve analysis)
	Quartz sand (QS)
Quartz powder (QP)	Specific gravity - 1.2 Particle size range - 400 μm to 800 μm Specific gravity - 2.61
	Quartz powder (QP)
Nano Silica (NS)	Particle size range - 2.3 μm to 75 μm Percentage of passing - 52% (45 μm sieve in wet sieve analysis) Appearance - White colour powder Particle Size - 10 nm to 20 nm
	Nano Silica (NS)
Steel Fibers	SSA - 600 m^2/g Density - 2.2 – 2.6 g/cm^3 at 25°C Purity - 99.5% Specific gravity - 7.8
	Steel Fibers
Super Plasticizers (SP)	Length - 13 mm Diameter - 0.18mm Yield stress - 1500 MPa Type - Polycarboxylate Ether Based Appearance - Light yellow coloured liquid
	Super Plasticizers (SP)
	pH - 6.5 Volumetric mass at 20°C - 1.06 kg/litre

mixes are given in Table 2. The materials and mix proportions used in the three high strength concrete (HSC) mixes are given in Table 3. To prepare the high strength concrete containing nano particles, first the binders such as cement and silica fume are added to quartz sand are dry mixed for 2 minutes in a hobart machine. The dispersed nano silica is added to the dry mix. The remaining water which was premixed with the superplasticizer was added and mixing is carried out for 5 minutes. The freshly prepared concrete is poured into moulds and after pouring, an external table vibrator is used to facilitate compaction and decrease the amount of air bubbles. The specimens are demoulded after a lapse of 24 hours and then cured under water at temperature of $20\pm 3^\circ\text{C}$. The compression and split tensile tests were carried out on cubic (70.7 mm) and cylindrical (50 mm×100 mm) specimens of the three HSC mixes. Table 4 gives the mechanical properties of the three HSC mixes. Notches (width approximately 3 mm) of various depths given

Table 3 Mix proportions by mass (except the steel fiber which is by volume) of three HSC

Mix ID	Cement	Silica fume	Quartz sand	Quartz powder	Nano silica	Steel fibre by vol. (length=13 mm, dia.=0.18 mm)	w/c	SP, %
HSC 1	1	0.25	1.5	-	2%	-	0.4	0.4%
HSC 2	1	0.25	1.1	0.4	2%	-	0.4	0.6%
HSC 3	1	0.25	1.1	0.4	2%	2%	0.4	0.6%

Table 4 Mechanical properties of Three HSC

Mix ID	Compressive strength (MPa)	Split tensile strength (MPa)
HSC 1	59.03	7.92
HSC 2	67.01	8.13
HSC 3	71.82	14.5

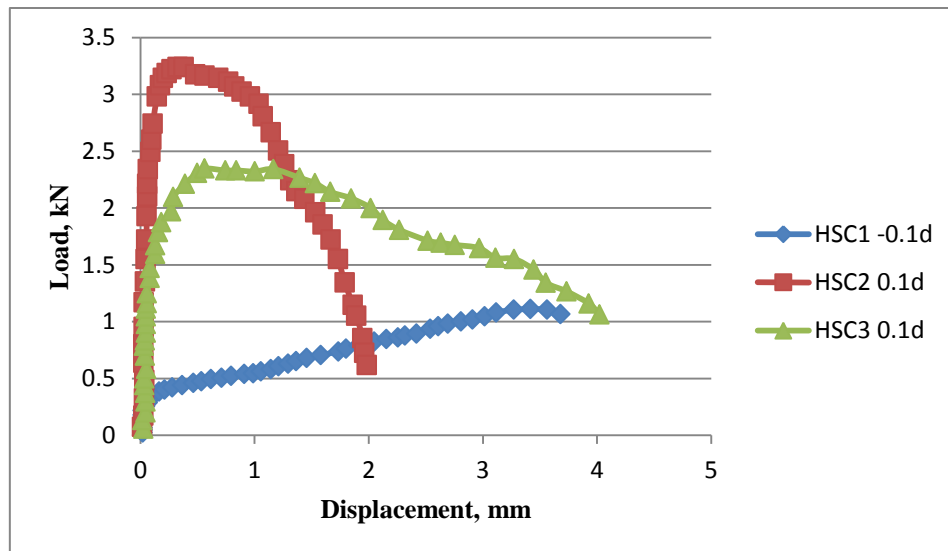


Fig. 7(a) Typical load vs displacement

in Table 1 were cut in beam specimens using a diamond saw. All tests were performed in a closed-loop servo-hydraulic testing machine, controlled by the crack mouth opening displacement (CMOD) measured with a clip gauge. A linearly varying displacement transducer (LVDT) was used to measure the mid-span vertical displacement, δ . The load-CMOD and load-displacement curves of all specimens were recorded. The ratio of the span between the supports to the depth of the specimen is maintained at 4 for all specimens. Fig. 7(a) shows typical load-deflection plot for HSC mix and Fig. 7(b) shows the typical failure of the specimen.

Table 5 shows size dependent fracture energy determined by RILEM work of fracture method G_f (i.e., Eq. (1) without the correction term for P - δ tail), the size-independent specific fracture energy (G_f) and G_F obtained by using simplified boundary effect method and Transition ligament length, a_l (mm). In the case of RILEM work of fracture method with P - δ tail correction, it is assumed to vary linearly from P to zero load and δ was computed using the known slope of the P - δ at δ_u from the recorded readings (refer Fig. 2). The simplified boundary effect method

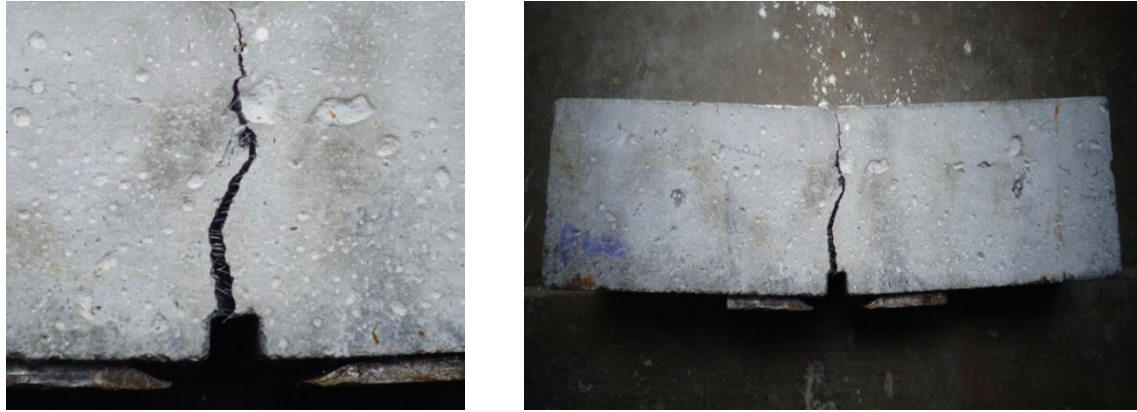


Fig. 7(b) Failure behaviour of specimen

Table 5 Size dependent fracture energy and size independent fracture energy for three HSC considering P - δ tail segment

Mix ID	Notch to depth ratio	G_f as per RILEM N/m	G_F (N/m) by				% diff compared to BEM
			RILEM G_f with P - δ tail segment,	RILEM G_f with P - δ tail segment (Average)	Boundary Effect Method (BEM)	Transition ligament length, a_l (mm)	
HSC 1	0.1	1059.25	1192.26	1173.08	1222.49	14.39	4.04
	0.6	855.56	1153.89				
HSC 2	0.1	1840.74	2065.15	2109.69	2260.39	20.04	6.67
	0.6	1316.67	2154.22				
HSC 3	0.1	2707.41	3345.89	3374.11	3566.71	26.22	5.40
	0.6	1633.33	3402.33				

proposed by Abdalla and Karihaloo (2003) has been employed to determine the G_F and transition ligament length a_l as the notch to depth ratios are well separated. Table 5 highlights the dependency of the RILEM specific fracture energy on the notch depth. The specific fracture energy decreases with an increase in the notch to depth ratio for the same beam depth. From Table 5, it is clear that G_F values are almost the same for a particular mix i.e., HSC1, HSC2, HSC3 irrespective of notch depth. Further, it can be noted that the G_F obtained from both the methods resulted in nearly same value. This important conclusion shows the further evidence that either of them can be employed for estimation of size independent fracture energy for analysis of cracked concrete structural components. It might appear at first sight that these two methods use very different experimental procedures, but in reality they are closely interrelated. Both procedures apply some corrections to the final part of the P - δ diagram in the work-of-fracture test (Vydra *et al.* 2012).

6. Bilinear tension softening diagram

Load-CMOD curves have been generated for various beams with different notch to

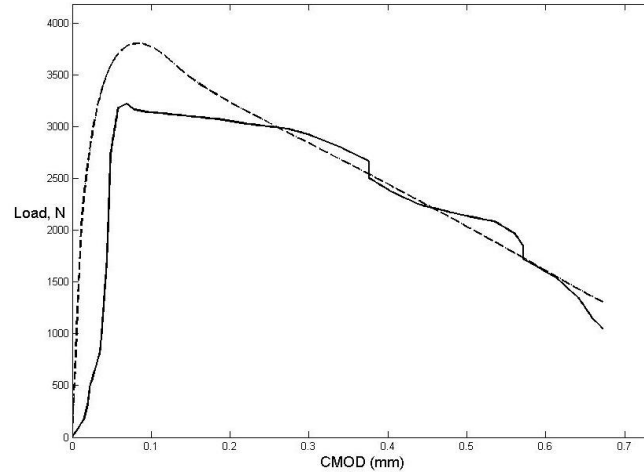


Fig. 8 Typical load-CMOD curve generated by the hinge model and average experimental load-CMOD curve

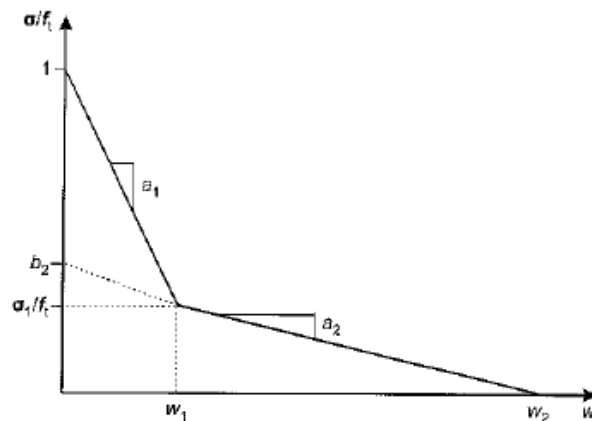


Fig. 9 Bilinear tension softening diagram

depth ratios. Fig. 8 shows the typical load-CMOD curves generated from hinge model and average experimental load-CMOD curve for HSC-3 with notch to depth ratio 0.1.

The area under the softening curve obtained by using the hinge model is not equal to G_F but to the measured $G_f(\alpha, W)$. It can be observed that the area under the bilinear TSD is generally less than the true G_F . Thus the true G_F of the HSC1, HSC2 and HSC3 1222.49 N/m, 2260.39 N/m and 3566.71 N/m respectively (Table 5) whereas the average area under the bilinear TSD is only 1173.08 N/m for the case of HSC1, 2109.69 N/m for HSC2 and 3374.11 N/m for HSC3.

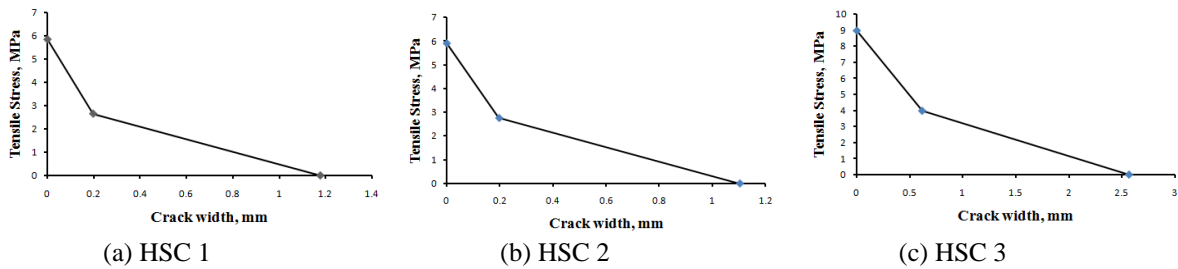
The size-dependent fracture energy (i.e., the area under the bilinear TSD) is given by (Fig. 9)

$$G_f^*(\alpha, W) = \frac{1}{2} f_t^* \left(w_1^* + \frac{\sigma_1^*}{f_t^*} w_2^* \right) \quad (9)$$

where the superscript * denotes the average parameters of the bilinear diagram obtained from the

Table 6 Parameters of the bilinear softening diagram corresponding to the size-independent fracture energy G_F

Mix	f_c , MPa	f_t , MPa	a_1 , mm ⁻¹	a_2 , mm ⁻¹	b_2	w_1 , mm	w_2 , mm	σ_1 , MPa
HSC1	59.03	5.84	2.769	0.452	0.532	0.202	1.176	2.65
HSC2	67.01	5.91	3.821	0.273	0.301	0.197	1.102	2.72
HSC3	71.82	8.96	0.791	0.264	0.676	0.615	2.564	3.97

Fig. 10 Bilinear stress-crack opening relationship for HSC1, HSC2 and HSC3 corresponding to their true fracture energy G_F

hinge model.

The size-independent fracture energy (i.e., the area under the bilinear TSD corresponding to G_F) can similarly be written as

$$G_F = \frac{1}{2} f_t \left(w_1 + \frac{\sigma_1}{f_t} w_2 \right) \quad (10)$$

where w_1 , w_2 and σ_1 , which are to be determined, are the bilinear diagram parameters corresponding to the true fracture energy G_F , and f_t is the direct tensile strength of the mix obtained from an independent test, say a split cylinder test, f_{st} .

The parameters of the bilinear TSD corresponding to the true G_F values of three concrete mixes have been obtained as per the procedure given by Abdalla and Karihaloo (2004) and are shown in Table 6. The TSDs are plotted in Fig. 10.

7. Conclusions

For the analysis of cracked concrete structures using the non-linear theory of fracture mechanics based on the fictitious crack model, two fracture properties of concrete are needed, namely, the specific fracture energy G_F and the corresponding tension softening relationship $\sigma(w)$. In this paper, the specific fracture energy by using two popular methods, namely, RILEM fracture energy with P - δ tail correction and simplified boundary effect method and corresponding bilinear approximation of the tension softening relation. From the above analysis of the experimental data on three grades of concrete ranging in compressive strength from 59 to 72 MPa the following conclusions can be drawn.

- In common with all previous investigations it has been found that the specific fracture energy G_f measured using the RILEM work-of-fracture procedure is highly dependent on the notch to

depth ratio. For the HSC1 used in the present investigation it varied between 855.56 N/m for $a/D=0.6$ to 1059.25 N/m for the same specimen with $a/D=0.1$ (Table 5). For the HSC2 (Table 5) it varied between 1316.67 N/m ($a/D=0.6$) and 1840.74 N/m ($a/D=0.1$) and for the HSC3 (Table 5) it varied between 1633.3 N/m ($a/D=0.6$) and 2707.41 N/m ($a/D=0.1$).

- The correction of the size-dependent G_f by the procedure proposed by Elices and his co-investigators (Elices *et al.* 1992, Guinea *et al.* 1992, Planas *et al.* 1992) or by the boundary effect procedure of Hu and Wittmann (2000) resulted in nearly the same size-independent G_f irrespective of the notch to depth ratio of the same specimen. For the HSC1, G_f is 1173.08 N/m by RILEM with P- δ tail correction and 1222.49 N/m by simplified boundary effect method (Table 5). For HSC2, the values are 2109.69 N/m and 2260.39 N/m and for HSC3, the values are 3374.6 N/m and 3566.71 N/m. The maximum difference between the values computed by using above mentioned methods for these three mixes is 6.67% (Table 5). This shows further evidence that either of the two procedures may be used in practice for analysis of cracked concrete structures. Karihaloo *et al.* (2003) and Ramachandra Murthy *et al.* (2013) have also shown that the size-independent specific fracture energy G_f of a concrete mix is also independent of the shape of the test specimen (notched three-point bend or wedge splitting) and not only its size and notch to depth ratio.

- The parameters of a bilinear approximation of the tension softening relation $\sigma(w)$ corresponding to the recorded load-CMOD diagrams of the TPB specimens have been inferred through an inverse analysis based on the concept of a non-linear hinge. But, these parameters are corresponding to specific notch to depth ratio of the specimen.

- However, when these parameters are appropriately scaled using the procedure proposed by Abdalla and Karihaloo (2004) so that they correspond to the size-independent G_f of the concrete mix, then these parameters are also independent of the specimen size and shape.

Acknowledgements

The authors thank the staff of the Computational Structural Mechanics Group and Advances Materials Laboratory of CSIR-SERC for their co-operation and suggestions provided during the investigations. This paper is being published with the kind permission of the Director, CSIR-SERC.

References

- Abdalla, H.M. and Karihaloo, B.L. (2003), "Determination of size-independent specific fracture energy of concrete from three-point bend and wedge splitting tests", *Mag. Concrete Res.*, **55**, 133-141.
- Abdalla, H.M. and Karihaloo, B.L. (2004), "A method for constructing the bilinear tension softening diagram of concrete corresponding to its true fracture energy", *Mag. Concrete Res.*, **56**, 597-604.
- Bazant, Z.P. and Kazemi, M.T. (1991), "Size dependence of concrete fracture energy determined by RILEM work-of-fracture method", *Int. J. Fract.*, **51**, 121-138.
- Bazant, Z.P. (1996), "Analysis of work-of-fracture method for measuring fracture energy of concrete", *ASCE J. Mater. Civil Eng.*, **122**, 138-144.
- Carpinteri, A. and Chiaia, B. (1996), "Size effects on concrete fracture energy: dimensional transition from order to disorder", *Mater. Struct.* **29**, 259-266.
- Cifuentes, H., Alcalde, M. and Medina, F. (2013), "Measuring the size independent fracture energy of

- concrete”, *Strain*, **49**, 54-59.
- Elices, M., Guinea, G.V. and Planas, J. (1992), “Measurement of the fracture energy using three-point bend tests: part 3-Influence of cutting the $P-\delta$ tail”, *Mater. Struct.*, **25**, 137-163.
- Karihaloo, B.L., Abdalla, H.M. and Imjai, T. (2003), “A simple method for determining the true specific fracture energy of concrete”, *Mag. Concrete Res.*, **55**, 471-481.
- Guinea, G.V., Planas, J. and Elices, M. (1992), “Measurement of the fracture energy using three-point bend tests: part 1-Influence of experimental procedures”, *Mater. Struct.*, **25**, 212-218.
- Hillerborg, A., Modeer, M. and Petersson, P.E. (1976), “Analysis of crack formation and crack growth in concrete by means of fracture mechanics and finite elements”, *Cement Concrete Res.*, **6**, 773-782.
- Hu, X. and Wittmann, F. (1992), “Fracture energy and fracture process zone”, *Mater. Struct.* **25**, 319-326.
- Hu, X. and Wittmann, F. (2000), “Size effect on toughness induced by crack close to free surface”, *Eng. Fract. Mech.*, **65**, 209-221.
- Jalal, M. (2014), “Corrosion resistant self-compacting concrete using micro and Nano silica admixtures”. *Struct. Eng. Mech.*, **51**, 403-412.
- Karihaloo, B.L. (1995), *Fracture Mechanics and Structural Concrete*, Addison Wesley Longman, UK.
- Mindess, S. (1984), “The effect of specimen size on the fracture energy of concrete”, *Cement Concrete Res.*, **14**, 431-436.
- Nallathambi, P., Karihaloo, B.L. and Heaton, B.S. (1985), “Various size effects in fracture of concrete”, *Cement Concrete Res.*, **15**, 117-126.
- Olesen, J.F. (2001), “Fictitious crack propagation in fiber-reinforced concrete beams”, *J. Eng. Mech.*, ASCE, **127**, 272-280.
- Ostergaard, L. (2003), “Early-age fracture mechanics and cracking of concrete”, PhD Thesis, The Technical University of Denmark, Lyngby.
- Pacheco-Torgal, F. and Jalali, S. (2011), “Nanotechnology: Advantages and drawbacks in the field of construction and building materials UK”, *Constr. Build. Mater.*, **25**, 582-590.
- Pan, Z. (2011), “Fracture properties of geopolymer paste and concrete”, *Mag. Concrete Res.*, **63**, 763-771.
- Planas, J., Elices, M. and Guinea, G.V. (1992), “Measurement of the fracture energy using three-point bend tests: part 2-Influence of bulk energy dissipation”, *Mater. Struct.*, **25**, 305-312.
- Ramachandra Murthy, A., Karihaloo, B.L., Iyer, N.R. and Raghu Prasad, B.K. (2013), “Determination of Size-independent specific fracture energy of concrete mixes by two methods”, *Cement Concrete Res.*, **50**, 19-25
- RILEM TCM-85 (1985), “Determination of the fracture energy of mortar and concrete by means of three-point bend tests on notched beams”, *Mater. Struct.*, **18**, 287-290.
- Sahin, Y. and Koksali, F. (2011), “The influences of matrix and steel fibre tensile strengths on the fracture energy of high strength concrete”, *Constr. Build. Mater.*, **25**, 1801-1806.
- Said, A.M., Zeidan, M.S., Bassuoni, M.T. and Tian, Y. (2012), “Properties of concrete incorporating nano-silica”, *Constr. Build. Mater.*, **36**, 838-844.
- Sanchez, F. and Sobolev, K. (2010), “Nanotechnology in concrete-A review”, *Constr. Build. Mater.*, **24**, 2060-2071.
- Singh, L.P., Karade, S.R., Bhattacharyya, S.K., Yousuf, M.M. and Ahalawat, S. (2013), “Beneficial role of nanosilica in cement based materials-A review”, *Constr. Build. Mater.*, **47**, 1069-1077.
- Stang, H. and Olesen, J.F. (1998), “On the interpretation of bending tests on FRC-materials”, *Proceedings of the FRAMCOS-3, Fracture Mechanics of Concrete Structures*, Aedificatio Publishers, Freiburg, Germany.
- Tabatabaei, R., Sanjari, H.R. and Shamsadini, M. (2014), “The use of artificial neural networks in predicting ASR of concrete containing Nano-silica”, *Comput Concrete*, **13**, 739-748.
- Tada, H., Paris, P.C. and Irwin, G.R. (1985), *The Stress Analysis of Cracks Handbook*, 2nd Edition, St. Louis MO, Paris Productions.
- Ulfkjaer, J.P., Krenk, S. and Brincker, R. (1995), “Analytical model for fictitious crack propagation in concrete beams”, *J Eng Mech.*, ASCE, **121**(1), 7-15.
- Vydra, V., Trtik, K. and Vodak, F. (2012), “Size independent fracture energy of concrete”, *Constr. Build. Mater.*, **26**, 357-361.

Zhang, P, Liu, C.H., Li, Q.F., Zhang, T.H. and Wang, P. (2014), "Fracture properties of steel fibre reinforced high-performance concrete containing nano-SiO₂ and fly ash", *Current Sci.*, **106**(7), 980.

CC